



Z. Broučková · Z. Trávníček

Intermittent round jet controlled by lateral pulse-modulated synthetic jets

Received: 6 November 2018 / Revised: 18 December 2018 / Accepted: 23 January 2019 / Published online: 19 February 2019
© The Visualization Society of Japan 2019

Abstract A round air jet was actively controlled by a pair of lateral control jets. The control jets were generated by a pair of opposing synthetic jet actuators, which were driven by the pulse-modulated sinusoidal signal. Two carrier frequencies were tested, namely 160 Hz and 840 Hz. Moreover, control jets driven by un-modulated sinusoidal signals were also tested. An unforced continuous jet was used as the reference case, and for all cases, the Reynolds number of the main round jet was 1570 (related to the nozzle exit diameter of 10 mm). Experiments (flow visualization and hot-wire anemometry) revealed that the flow control caused a suppression of the jet core and a more rapid jet flow decay. In addition, the pulse modulation caused jet intermittency that was distinguished by the periodicity of the time-averaged and fluctuating velocity components. For the case of the lower carrier frequency of 160 Hz, a flapping motion of the controlled jet occurred and the jet formed a zigzag pattern.

Keywords Flow control · Pulse modulation · Synthetic jet · Flow visualization · Hot-wire anemometry

1 Introduction

Fluid jet flows, an important case of fluid motion, have been frequently employed in various industrial processes. A majority of jet flow studies, as well as the applications, deal with continuous jets at steady-state flow conditions; however, the increasing opportunities associated with jet flows are linked to their enhancement by flow unsteadiness.

This study focuses on submerged fluid jets for which the properties of the working fluid are similar to those of the surroundings. Its counterpart is the free-surface jet (typically a water jet in air), which is mentioned here to illustrate a very representative type of discontinuous jet, namely the mechanically intermittent water jet. Zumbrunnen and Aziz (1993) created an intermittent free-surface planar water jet using a blade wheel penetrating the jet trajectory. Such mechanical devices seem to be the most illustrative for the demonstration of the various means of introducing fluid oscillations into the fluid flow.

Examples in which fluid flows are periodically cut off include the use of evenly rotating valves inserted into the fluid supply, see, e.g., Azevedo et al. (1994) and Mladin and Zumbrunnen (1997). A highly sophisticated electromechanical mass flow rate control system was developed by Durst et al. (2003); the system was intended for laboratory experiments with unsteady flows with (nearly) arbitrary waveforms up to a frequency of 125 Hz. Reynolds et al. (2003) proposed another mechanical method, based on a combination of two mechanical actuations with an adjustable phase shift (namely an orbital wobbling nozzle and axial

vibrations). These authors demonstrated that very complex three-dimensional jet flows, such as bifurcating, trifurcating, and blooming jets, can be created in this way.

A great advantage of such mechanical devices typically seeks to predict, with an adequate accuracy, the characteristics of the flow unsteadiness. On the other hand, many disadvantages occur as a result of moving components. Therefore, a utilization of fluidics principles (flow handling without the action of moving components) may be a promising alternative. A relevant method might be based on self-sustained oscillations; for example, the self-oscillating flapping jet can be driven by the feedback loop of a fluidic oscillator, as proposed by Viets (1975) and investigated in the studies of Raman et al. (1994) and Camci and Herr (2002). Two different fluidic variants were investigated by Mi et al. (2001). The first is a flapping jet nozzle that generated a two-dimensional flip–flop motion of the entire jet with respect to the major plane of symmetry of the rectangular nozzle. This method resembles that of Viets (1975); however, the mechanism is different because it needs neither an external trigger nor any external feedback tube. The second variant is the precessing jet nozzle, which utilizes an instability of large-scale precessing flows within a cylindrical chamber downstream of a sudden expansion, as was explained by Nathan et al. (1998).

Another variant was proposed by Hsiao et al. (1999): A circular cylinder was placed into the potential core of a plane air jet with an aspect ratio of 20 at the nozzle exit. Self-sustained oscillations in the flow were experimentally evaluated and the complexities of the fluid dynamics were discussed with respect to the jet-on-cylinder impingement, shear layer instability, and cylinder wake shedding. A seemingly similar, but in fact more complicated, mechano-fluidic method was proposed by Haneda et al. (1998). Unlike a fixed support of the cylinder by Hsiao et al. (1999), Haneda et al. (1998) used an elastic support. An elastically supported circular cylinder was placed into the potential core of a plane air jet (aspect ratio of 33 at the nozzle exit). An aeromechanical coupling of the vortex shedding from the cylinder with the mechanical cross-stream oscillations of the cylinder (resulting from its elastic support) caused a desirable actuation of the main jet flow.

A self-oscillating axisymmetric jet, generated by means of a collar that extended the pipe nozzle exit (the so-called whistler nozzle), was developed by Hill and Greene (1977). Hussain and Hasan (1983) proposed an explanation for the phenomenon, highlighting the coupling of two independent resonance mechanisms, namely the organ pipe resonance and the shear layer tone resulting from the pipe-exit shear layer impinging on the collar lip. Note that this type of geometry was utilized by Page et al. (1996) to obtain an enhancement means of impingement heat transfer.

Another method for the generation of periodical structures in jet flows uses vortex shedding from an obstacle inserted into the jet flow; thus, a continuous jet is actuated by the periodic wake formed downstream of a bluff body submerged in the jet. For example, Herwig et al. (2004) proposed three different variants of the self-sustained periodical jet: The first variant (called the “Karman jet nozzle”) used an axisymmetric nozzle with a ring obstacle inserted into the nozzle exit, the second used a fluidic flip–flop oscillator, and the third used a precessing jet (Nathan et al. 1998). The aim was to achieve augmentation of the impingement-related heat transfer and, while successful, the power increase required to overcome the blockage effect of the obstacles in the experiment was not discussed by Herwig et al. (2004).

Because devices based on the fluidics principles do not require moving parts, they are quite attractive. A reduction in, or even elimination of, mechanically movable elements is desirable for cost-effective operation as well as user-friendly control. However, at least two disadvantages should be mentioned here. The first is that the self-sustained oscillation process can consume too much of the energy of the mean flow. The second is that the flow characteristics are largely predetermined by the geometry and cannot be easily controlled by changing the conditions. This can be a serious disadvantage in test use for research purposes. Considering that a combination of positive features from various methods can be advantageous, conventional jet flows can be controlled (vectored) by various lateral control jets.

For example, Favre-Marinet et al. (1981) developed a method for generating flapping jets by means of a pair of lateral control pulsating jets vectoring the central main jet flow. Control pulsations were created by means of periodic termination of the air supply flowing through a pair of rotating cylindrical valves. Other examples of laterally influencing control jets are discussed in the studies of Tamburello and Amitay (2007a, b). The lateral control jets were either continual jets (2007a) or synthetic jets (2007b).

The synthetic jet (SJ) is a type of pulsating jet flow that is created during the oscillatory process of fluid exchange between an actuator cavity and its surroundings (Smith and Glezer 1998; Glezer and Amitay 2002; Mohseni and Mittal 2015). The flow through the cavity orifice is reciprocating in character; therefore, SJ is also commonly known as the zero-net-mass-flux jet (Cater and Soria 2002; Pack and Seifert 2001). SJs have many potential applications, typically aimed at active flow control such as jet vectoring and flow control in

external/internal aerodynamics. Other potential fields of application include convective heat transfer for the cooling of electronic components and turbine blades, mass transfer enhancement, and thrusters for underwater vehicles. The area that is most relevant to this study is jet vectoring (Tamburello and Amitay 2007b; Pack and Seifert 2001; Smith and Glezer 2002; Ben Chiekh et al. 2003).

The switching of an actively controlled flip–flop jet was investigated recently, aiming to enhance impingement heat transfer—see (Trávníček et al. 2003, 2014). The main annular jet was controlled by lateral control jets, which were either continuous jets (2003) or SJs (2014).

A driving signal in a majority of the studies concerning SJs has a sinusoidal waveform; however, it appears that it may sometimes be more beneficial to use non-sinusoidal ones, see Zhang and Wang (2007) and Kordík and Trávníček (2018). Other possibilities are linked with the utilization of various modulated signals (Tamburello and Amitay 2007b; Qayoum et al. 2010). The aim of the present study is to demonstrate a versatile and flexible alternative for the generation of intermittent jet flows by means of active flow control. For this reason, pulse-modulated synthetic jets are used as the control tools, and this study presents the proposed alternative, demonstrated with the use of flow visualizations and hot-wire measurements.

2 Experiments

2.1 Experimental setup and measurement techniques

The scheme of the investigated device, including the coordinate system, is shown in Fig. 1. The device is a modified version of a previous variant that was designed for the investigation of actively controlled impinging jets, see Trávníček et al. (2012).

The working fluid is air. The main air flow (position 1 in Fig. 1) is supplied by a compressor and passes through the grid (2), settling chamber (3a), honeycomb (4), and the second settling chamber (3b) to the quadrant-contoured nozzle (5) generating the main jet. The exit diameter and the area contraction ratio are $D = 10$ mm and $\varepsilon = 21.2$, respectively. The exit channel of the nozzle is a short cylindrical pipe (of 13 mm length) with a constant cross section of 10 mm diameter.

The exit of the main jet nozzle is equipped with two actuators (6a, 6b), denoted L (left) and R (right) in Fig. 1. Both actuators are driven electro-dynamically by diaphragms that originated from loudspeakers (Monacor SP-7/4S). Both actuators are able to generate the SJs. The exits of both of the actuators consist of rectangular slot nozzles of 1.1×6 mm (7a, 7b), which are laterally oriented with respect to the primary jet axis. The cavities of the actuators are connected to their exit slots by pipes of inner diameter and length of 9.2 mm and $l = 63$ mm, respectively. Both the L- and R-actuators are electrically anti-series connected, i.e., they run in opposite directions, and are fed from the sweep/function generator (Rigol DG4062) which is amplified by the audio amplifier (PIONEER A-209R). The input peak-to-peak voltage is maintained at 4.8 V for each actuator.

Two experimental methods were applied in this study: qualitative flow visualization and quantitative measurement using the hot-wire anemometry technique. The flow visualization was performed using water fog, which was added into the main air jet supply, and in phase-locked regime under the stroboscopic light (Cole Parmer U-87002-35). A moderate backlight effect was used to enhance an image contrast of water fog contours; hence, the angle between the camera and light directions was approximately 110° (Fig. 1b). The flash duration was $1\text{--}3 \times 10^{-5}$ s, which can be considered as an instantaneous flash relatively to the present driving signals. To demonstrate the flash shortness, it can be compared with the control signal, which will be described in the following text (summarized in Table 1 and shown in Fig. 3). The mentioned flash duration is represented in Fig. 3 as a time window (streak) narrower than 0.06 mm. The stroboscopic light was synchronized with the driving signal at a chosen phase shift. The pictures were taken using a digital camera connected to a PC via a USB. The exposure time was 1–1.5 s, so that the resulting pictures are in fact multi-exposures of many (tens or hundreds) working cycles. Therefore, the pictures show the phase-locked feature of the flow field, while random disturbances in the individual cycles are smoothed out.

A hot-wire anemometer (MiniCTA 55T30, Dantec Dynamics) with a single-wire probe (55P16) together with a data acquisition device NI PCI-6023E was used for velocity measurement in constant temperature (CTA) mode. A typical sampling frequency and number of samples were 5–10 kHz and 16,384, respectively. For the present experiments, the anemometer was calibrated in the velocity range approximately from 0.5 to 20.5 m/s, and the linearization error of the calibration (using a four-degree polynomial) was within 2%. Temperature measurement using a fast response temperature system 54T40 with a thermistor probe

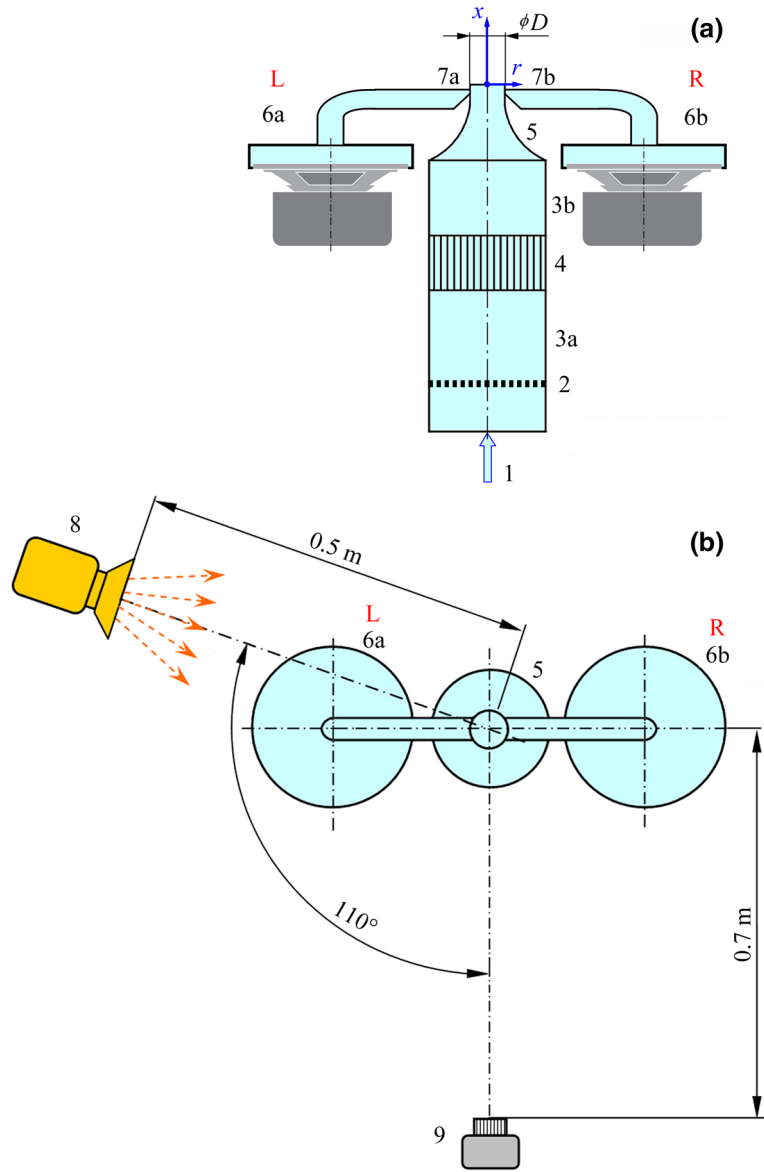


Fig. 1 Schematic view of the investigated configuration (drawing not to scale): **a** front view, **b** top view, 1: primary air flow supply, 2: grid, 3a and 3b: settling chambers, 4: honeycomb, 5: contoured contraction, 6a and 6b: SJ actuators; 7a and 7b: control slot nozzles; 8: stroboscope; 9: camera

Table 1 Parameters of the control jets

Case	Modulation frequency		Number of pulses N	Duty cycle		
	f (Hz)	f_{mod} (Hz)		D_c (%)	U_0 (m/s)	$U_{0,\text{mod}}$ (m/s)
1. Pulse-modulated SJs (Fig. 3a)	160	20	1	12.5	–	0.24
2. Standard SJs	160	–	–	–	1.94	–
3. Pulse-modulated SJs (Fig. 3b)	840	28	4	13.3	–	0.49
4. Standard SJs	840	–	–	–	3.68	–
5. Without control jets (reference case)	–	–	–	–	–	–

(90P10) was used for the temperature correction of the hot-wire data. The velocity components are defined as follows: $u = U + U_p + u'$, where u is the instantaneous velocity and U , U_p , and u' are the time-averaged, periodic (phase locked, coherent), and fluctuating (incoherent, random) components, respectively.

Simultaneously with the hot-wire signal, the driving signal for the loudspeakers was recorded. Data post-processing was performed in MATLAB software by means of the phase-averaging and time-averaging procedures, and the number of cycles of the phase-averaging procedure was 46–65 cycles of the modulation signal.

The characteristic velocity of the main jet was evaluated as the area-averaged velocity from the axisymmetric velocity profile at the exit plane of the nozzle, $U_m = \frac{8}{D^2} \int_0^{D/2} u r dr$, where u is the local velocity. In this study, all experiments were performed at a velocity of $U_m = 2.5 \text{ ms}^{-1}$. The corresponding Reynolds number was $Re = U_m D / \nu = 1570$, where ν is the kinematic viscosity.

2.2 Frequency characteristics of the actuators and driving signals

The main round jet is vertically oriented and the control jets are generated from the control slot nozzles (7a, 7b in Fig. 1), which are laterally arranged. The SJ actuators can effectively operate at the resonance (Smith and Glezer 1998; Mohseni and Mittal 2015; De Luca et al. 2014; Kordík and Trávníček 2017).

To quantify the resonant frequencies for the present L- and R-actuators, the time-averaged velocity was measured downstream of the control nozzles, at the main nozzle axis at $r = 0$. The measurements were taken when the L- and R-actuators were operated separately. Figure 2 shows the frequency characteristics in the form of the time-averaged velocity versus the driving frequency. The curves obtained for the L- and R-actuators are similar in character, and the magnitudes of the maxima are also similar. Two resonances are revealed, with related resonant frequencies of approximately 40–100 Hz and 840–900 Hz. To obtain an efficient performance of the actuators, the carrier sinusoidal signal was chosen at 840 Hz. To complete this study with a low-frequency area, the second carrier signal was chosen at 160 Hz, despite the fact that it generates only approximately half of the velocity magnitude, as indicated in Fig. 2.

Another important factor, which was considered at the time of choice of the driving signal, is the sensitivity of the main round jet to external excitations. The most amplified mode is characterized as the most preferred mode by Crow and Champagne (1971) at a Strouhal number of 0.3, where the Strouhal number is defined as $St = f^* D / U_m$, where f^* is the relevant frequency. Note that natural passage frequencies of vortices in jet shear layers without any artificial excitation cover usually a wider range of the Strouhal numbers from 0.25 to 0.85, as was concluded by Thomas (1991).

For the particular case of the present quadrant-contoured nozzle (Fig. 1), the natural passing frequency of the vortices in an unforced jet was evaluated at $Re = 1600$ to be $f^* = 58.6 \text{ Hz}$ which yields $St = 0.24$, see Trávníček et al. (2012). Therefore, the modulation frequencies in the present study are chosen to be in the range $f_{\text{mod}} = 20\text{--}28 \text{ Hz}$ (i.e., $St = 0.08\text{--}0.11$), which is slightly below the subharmonics of the natural passage frequencies.

The chosen variants of the control signal are summarized in Table 1 and shown in Fig. 3, where the voltage signal, V , is related to the voltage maximum $V_{\text{max}} = 2.4 \text{ V}$, which is half of the peak-to-peak voltage of 4.8 V:

- Cases 1 and 3: The main topic of this study focuses on pulse-modulated control signals. Namely, the driving signal is the modulated sinusoidal signal with carrier frequencies of $f = 160 \text{ Hz}$ and 840 Hz and modulation (repetition) frequencies of $f_{\text{mod}} = 20$ and 28 Hz . The number of pulses (bursts) was chosen as $N = 1$ or $N = 4$ (Table 1 and Fig. 3).

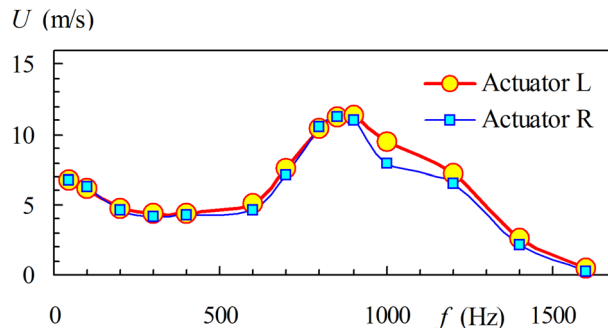


Fig. 2 Frequency characteristics of L- and R-actuators

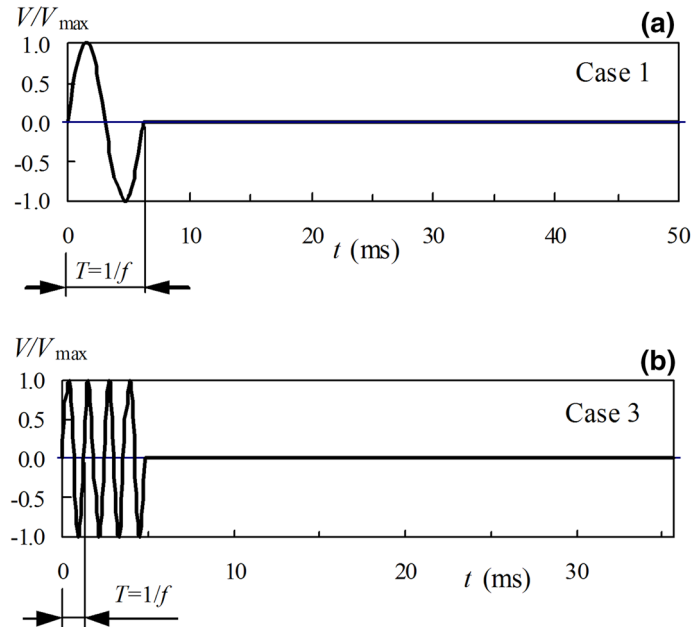


Fig. 3 Pulse-modulated driving signal of **a** Case 1 and **b** Case 3; parameters are summarized in Table 1

- Cases 2 and 4: For comparison purposes, standard SJs (i.e., without modulation) were also used as the control jets. In fact, these variants follow recent investigations revealing some positive features of the controlled jet for impingement heat/mass transfer enhancement, see Trávníček et al. (2012).
- Case 5: As the reference, an unforced continuous jet was used.

3 Results and discussion

3.1 Control jets

Figure 4 shows the results of two preliminary experiments demonstrating the behavior of both control jets, L and R. The measurements were taken separately for each actuator. The hot-wire probe was placed near the actuator orifice (about 0.5 mm downstream of the orifice, at $x = -2$ mm) and only one actuator was supplied with the driving pulse of Case 1 (Table 1). This pulse is also shown in Fig. 4, while the input peak-to-peak voltage of 4.8 V is not shown in the scale. The polarity was chosen so that the start of the pulse caused the extrusion stroke. Figure 4 shows the results: The differences between the waveforms are almost negligible; thus, it can be concluded that the control jets are very similar and that any differences in the individual properties of the L- and R-actuators are negligible.

Note that the character of the reciprocating velocity was considered for this presentation, i.e., the positive (extrusion) and the negative (suction) flow orientations were assumed and the velocities during the suction stroke were inverted. This de-rectification method is commonly used for SJ hot-wire data processing, see Smith and Glezer (1998), Broučková and Trávníček (2015), and Feero et al. (2015).

Sequentially, both of the control jets were tested with respect to the polarity of the anti-series connection; hence, the L- and R-actuators ran in opposite directions. Namely, the L-actuator always began its working cycle with an extrusion stroke, while the R-actuator began the suction stroke at the same moment. To quantify this process, the hot-wire probe was placed close to the L-actuator exit ($r = -4.5$ mm, $x = -2$ mm) and the L-actuator was turned on while the R-actuator was turned off. Figure 5 shows the resulting phase-averaged velocities. The input driving signal is also shown in Fig. 5. The parameters of Case 1 were the same as those discussed in Fig. 4.

After this experiment, the configuration was turned over and the hot-wire probe was placed close to the turned-on R-actuator ($r = +4.5$ mm, $x = -2$ mm). The resulting phase-averaged velocities are shown in Fig. 5. Obviously, the velocity waveforms of the L-actuator are the same in both Figs. 5 and 4, because they

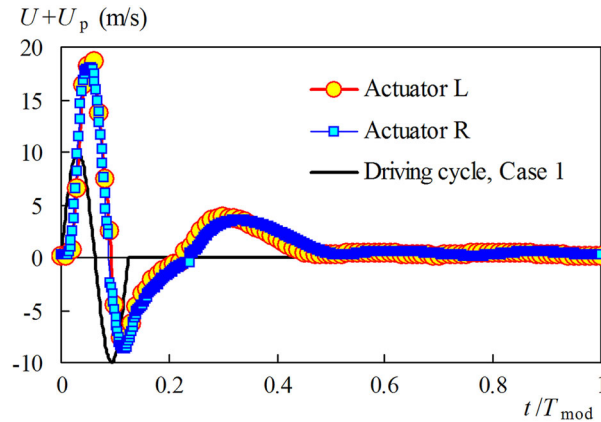


Fig. 4 Hot-wire measurements of both control jets, which were generated separately either from L- or R-actuator

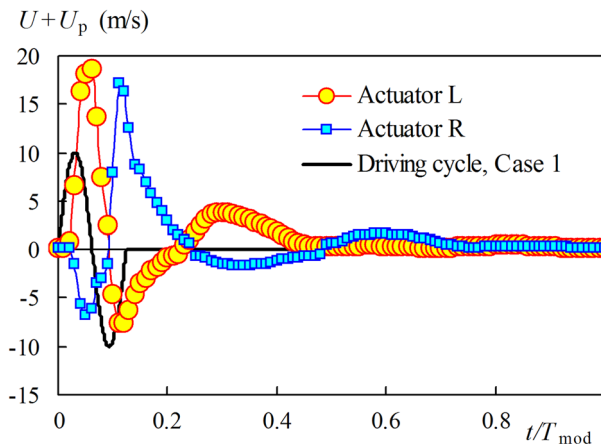


Fig. 5 Hot-wire measurements of both control jets, which were generated separately either from L- or R-actuator, with respect to the polarity of anti-series connection

are the result of repeated measurements. On the other hand, the velocity waveform of the R-actuator differs because of its opposite polarity: Shortly after the beginning of the working cycle, the air is extruded from the orifice of the L-actuator and it is sucked during the following part of the cycle. The R-actuator works in the opposite direction, i.e., it starts with the suction stroke.

Although the driving pulse signal is limited to only one sinusoidal wave, the velocity waveforms of both jets present subsequent impulse tails, which are caused by the unavoidable tail oscillations of the driving diaphragms (Fig. 5).

It is worth noting here that differences in the character of the waveform of the L- and R-jet are not caused by any differences in the actuators. As confirmed in the text above, both actuators have virtually identical individual properties (Figs. 2 and 4). Moreover, the maximum velocities of 17–19 m/s are similar for both control jets (Fig. 5). Thus, the differences between the extrusion and suction waves in Fig. 5 can be attributed to nonlinearities in the reversed extrusion/suction movements of the entire dynamical system, as was analyzed in more detail by Kordík et al. (2014).

Figure 6 demonstrates the phase-averaged velocity magnitudes of the control SJs measured at the axis ($r = 0$ mm, $x = -2$ mm) for Case 1. Firstly, both of the SJs were investigated separately, see the L and R lines in Fig. 6. During the first half of the input pulse, the fluid is extruded from the L-actuator, and during the second half of the pulse, the fluid is extruded from the R-actuator. The secondary peaks caused by the tail oscillations are still discernible, as in Figs. 4 and 5.

The results when both actuators are turned on are marked as the “Actuator L and R” line in Fig. 6. The resulting velocity seems to be an envelope of the single velocity signals. Due to the interaction of the extruded fluid on the nozzle axis, the maximum obtained velocity peaks are slightly higher than those for the single SJ cases of L and R lines.

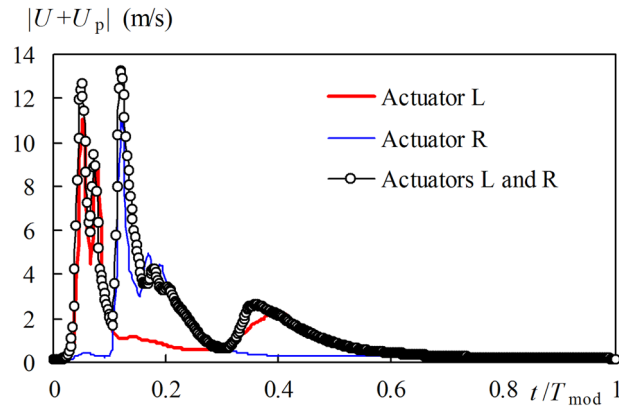


Fig. 6 Phase-averaged velocity magnitudes of control SJs measured at the axis ($r = 0$ mm, $x = -2$ mm) for Case 1

Similar experiments as discussed for Case 1 in Figs. 5 and 6 were conducted for a higher-frequency actuation, Case 3, i.e., at $f = 840$ Hz, $f_{\text{mod}} = 28$ Hz, and $N = 4$ (Table 1 and Fig. 3). The results are shown in Figs. 7 and 8. Again, the periodic movement of the loudspeaker's diaphragm causes periodic suction and extrusion through the exit orifices of the actuators which again work in opposite directions (Fig. 7). The tail oscillations are also easily distinguishable. The region of smaller secondary oscillations is visible in the second half of the cycle at $t/T_{\text{mod}} = 0.5\text{--}0.7$ in Fig. 7a. Very likely these oscillations indicate a reflection of

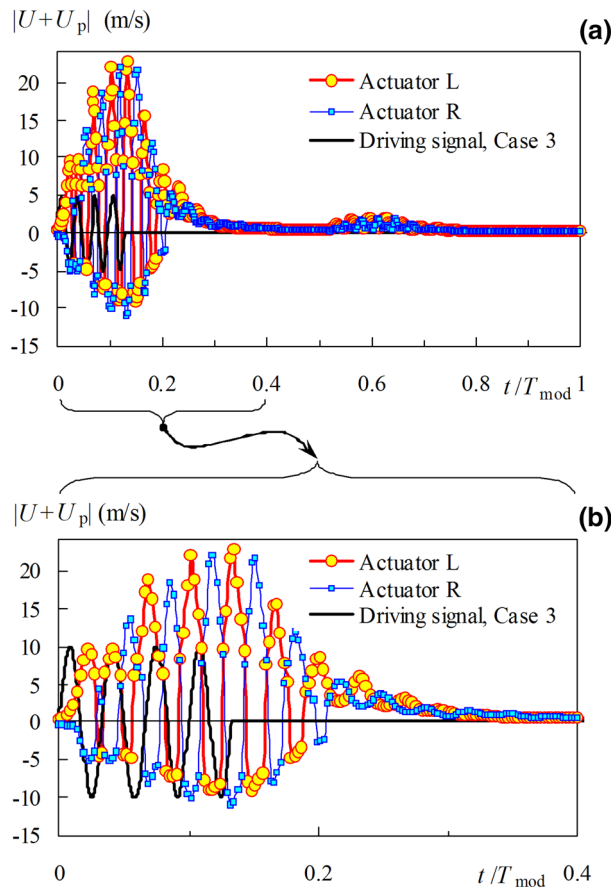


Fig. 7 Phase-averaged velocity magnitudes of both control jets, which were generated separately either from L- or R-actuator, with respect to the polarity of anti-series connection, for Case 3, **a** entire working cycle, **b** detail of pulses

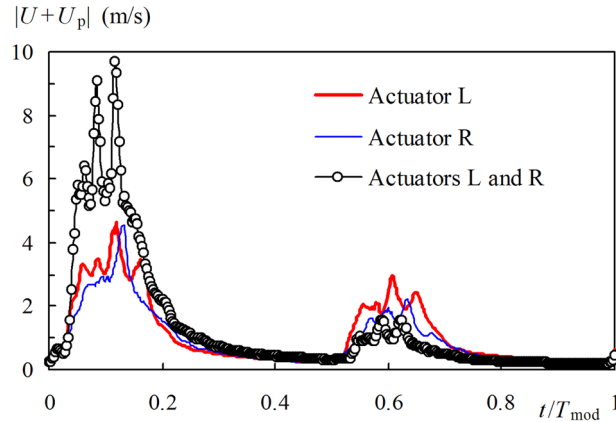


Fig. 8 Phase-averaged velocity magnitudes of control SJs measured at the axis ($r = 0$ mm, $x = -2$ mm) for Case 3

the extruded air puff train from the opposite wall of the nozzle. For the sake of clarity, the first part of the working cycle is shown in detail in Fig. 7b.

Measurements at the nozzle axis, shown in Fig. 8, indicate that the control jets interact in Case 3 more than the single-pulse jets of Case 1 shown in Fig. 6. The velocity waveforms of the single L- and R-jets are similar (shape of the waveform, maximum velocity, occurrence of the velocity peaks at the cycle beginning at $t/T = 0.05$ – 0.16). A region of increased velocity, occurring at $t/T = 0.55$ – 0.7 , is distinct; as stated above, this effect probably indicates a reflection of the jet from the opposite nozzle wall.

On the other hand, two characteristic differences in the velocity cycles are evident from a comparison of Figs. 6 and 8. Firstly, the “L and R” waveform for both of the operating jets in Fig. 6 seems to be an envelope of both single-jet waveforms; on the other hand, Fig. 8 indicates that the interaction of several extruded vortex puffs causes significant growth of the maximum velocity at the nozzle axis (synergy effect).

The second meaningful difference is a distinguishable character of the two velocity peaks in Fig. 6 (resulting from the extrusion strokes of the L- and R-actuators) versus the indistinguishable peaks in Fig. 8. The reason for this can be attributed to the interactions of the velocity peaks in a rather confined space inside the main nozzle.

To quantify the velocities of the control jets, the time-averaged extrusion velocity was experimentally evaluated. For conventional SJs (i.e., without modulation), the hot-wire probe was placed near the L- and R-actuator exits at $r = \pm 4.8$ mm, $x = -2$ mm. The instantaneous velocity in time, $u_0(t)$, was measured and the characteristic velocity, U_0 , was evaluated as the time-averaged velocity using the following formula:

$$U_0 = \frac{1}{T} \int_0^{T_E} u_0(t) dt, \quad (1)$$

where $T = 1/f$ is the duration of one period and T_E is the duration of the extrusion part of the cycle.

An evaluation of the characteristic velocities of the pulse-modulated jets was then made from the values of non-modulated SJs of the same frequency according to $U_{0,\text{mod}} = U_0 D_c$, where D_c is the duty cycle. The results are summarized in Table 1.

3.2 Flow visualization

Visualization of an unforced continuous jet issuing from a nozzle similar to that employed here (Fig. 1) was previously performed by Trávníček et al. (2012), revealing the natural passing frequency of the vortices to be $f^* = 58.6$ Hz, i.e., $St = 0.24$. Due to the rather low Reynolds number, the flow in the nozzle is laminar; however, it undergoes transition to turbulence shortly beyond the nozzle exit. This is in accordance with the conditions known to be necessary for the laminar regime of submerged axisymmetric jet flows, see, e.g., Bejan (1995).

The situation changes considerably when the control jets are applied. The evolution of the controlled main jet at several phases during the working cycle is illustrated in Fig. 9. The parameters of the control jets are specified as those of Case 1 in Table 1. The beginning of the working cycle, i.e., the part of the cycle at

which the control pulse jets are applied, $t/T_{\text{mod}} = 0$, is presented with a phase step of $t/T_{\text{mod}} = 0.042$ (i.e., a phase angle step of 15°) from $t/T_{\text{mod}} = 0$ to 0.125 . The remaining part of the cycle is presented with a step of 0.125 (i.e., 45°).

The influence of the control jets on the main jet is obvious: The main jet is at first directed to the right-hand side as the L-actuator begins its working cycle with an extrusion. Subsequently, the main jet is directed back to the left-hand side as the R-actuator starts its extrusion phase at $t/T_{\text{mod}} = 0.0625$ (i.e., at 22.5° , see Fig. 3). Therefore, the main jet forms a flapping zigzag pattern. The impact of the control jets is connected with the creation of the vortex structures on both sides of the main jet. The tail oscillations cause the evolution of smaller, secondary vortex structures on both sides of the jet. When the control effect subsides, the jet becomes calm and smooth and, in particular, at the end of the cycle the near-field character of the jet resembles an unforced, continuous jet, see the last image of Fig. 9 relating to $t/T_{\text{mod}} = 0.875$ (i.e., 315°).

To compare the effect of pulse modulation with control using standard SJs, visualization was also undertaken for Case 2 from Table 1. Figure 10 shows the resulting pictures at the time of the maximum extrusion velocity of the L-actuator and the maximum extrusion velocity of the R-actuator, i.e., at $t/T = 0.25$ and 0.75 , respectively. The jet differs in character from Case 1 with the pulse modulation shown above. Now, the jet spreading seems to be more uniform during the cycle, excepting the changes in the vicinity of the nozzle at $x/D < 1.2$, resulting from the culminations of the extrusion/suction strokes. The jet intermittent

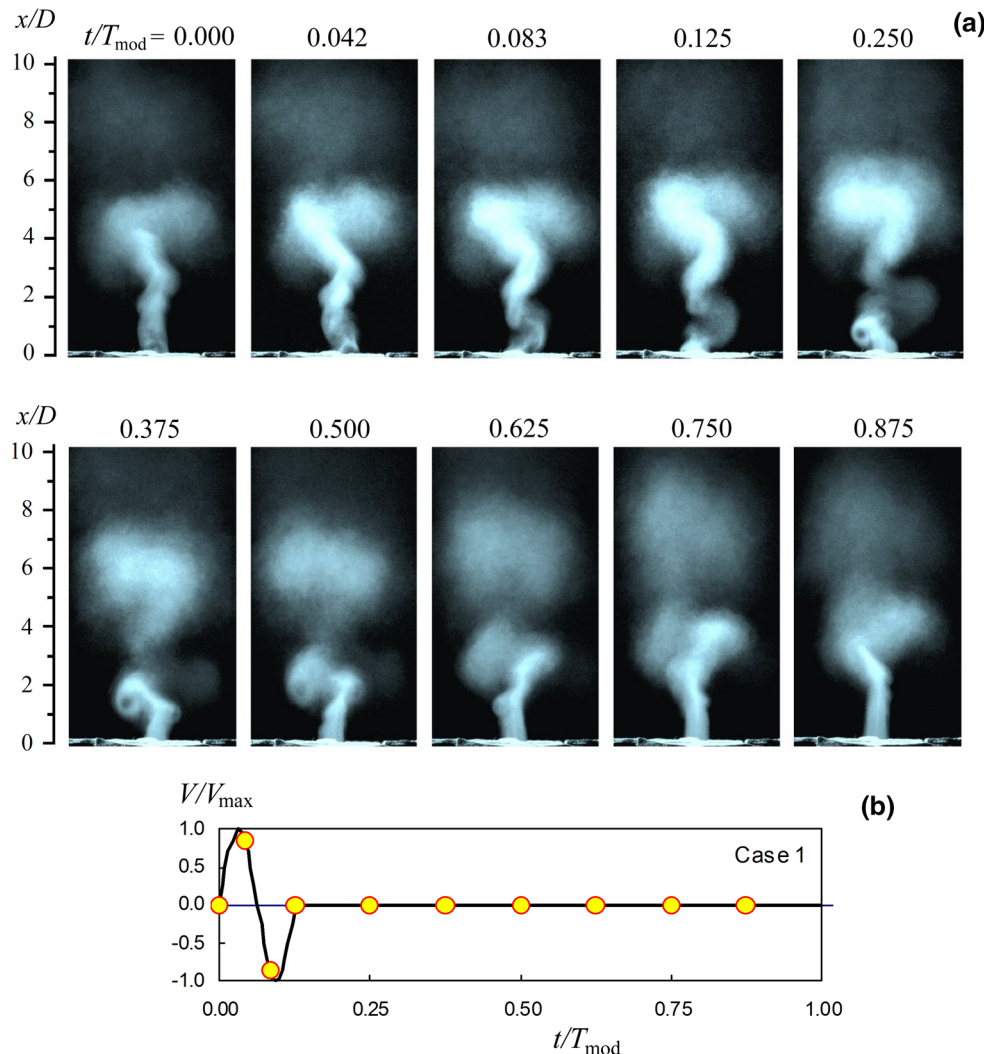


Fig. 9 **a** Phase-locked visualization during the actuating cycle for Case 1; parameters are summarized in Table 1; **b** driving signal with marks indicating phases of the visualizations

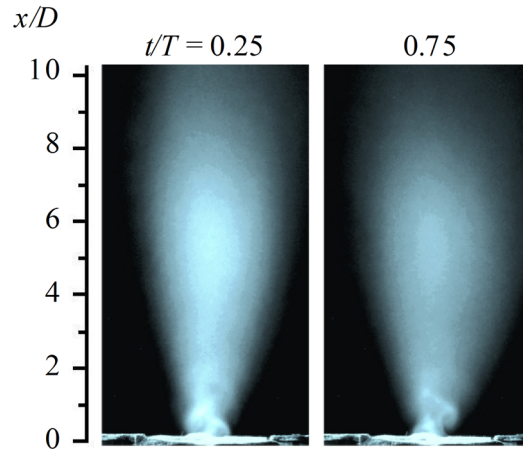


Fig. 10 Phase-locked visualization during the actuating cycle for Case 2; parameters are summarized in Table 1

character and the flapping zigzag pattern, resulting from pulse modulation in Case 1 (Fig. 9), are not observed with Case 2 (Fig. 10).

Figure 11 presents the evolution of the controlled main jet for Case 3 from Table 1. The images were taken at the same phases as was the case in Fig. 9. Evidently, the four control pulses of Case 3 bring about a more symmetrical jet flow, without any flapping motion or zigzag tendency, when compared to the effect of the single-pulse control jet of Case 1 shown in Fig. 9. Nevertheless, jet periodicity during the driving cycle can be recognized in the form of structures traveling along the jet axis.

For comparison purposes, Fig. 12 shows the flow visualization results for Case 4. Similar to Fig. 10, the jet is shown at the maximum extrusion velocities of the L-actuator and R-actuator ($t/T = 0.25$ and 0.75 , respectively). Similar to Fig. 10, the character of the jet is almost the same as that of Case 2 in Fig. 10.

The present visualizations demonstrate that pulse modulation of the control signal leads to a basically different behavior of the main jet. To quantify this effect, the results of the hot-wire measurements are presented in the following section.

3.3 Jet flow formation

Figure 13a shows the evolution of the time-averaged velocity of the main jet along the axis ($r = 0$). The behaviors of the forced jets of Cases 1 and 2 are compared with the reference unforced jet (Case 5), with the corresponding fluctuating velocity component u' (RMS, root mean square) shown in Fig. 13b. The results are presented in dimensionless form, namely $U/U_{0,N}$ and $u'/U_{0,N}$, respectively, where $U_{0,N}$ is the centerline time-averaged velocity at the nozzle exit.

The behavior of the reference unforced jet (Case 5) is typical for a jet issuing from a round nozzle; the velocity is constant until the end of the potential core at $x/D = 6-7$, at which point the velocity gradually decreases with a slope of $U \sim x^{-1.1}$. The magnitude of the exponent is somewhat higher than that usually stated ($U \sim x^{-1}$) for turbulent jets, see, e.g., the correlation of $U/U_{0,N} = 6 D/x$ by Blevins (2003), which is also presented in Fig. 13a. The reason for the slightly higher magnitude of the exponent may be related to the relatively short exit channel of the nozzle and the flow disturbances generated from the edges of the control nozzles, which can be considered as a passive effect which occurs even without the active control. The development of the fluctuation velocity component of the unforced Case 5 is shown in Fig. 13b: It is approximately constant ($u'/U_{0,N}$ is about 0.02) up to an area of $x/D \sim 1$. Further downstream, the fluctuations gradually increase to the local maximum ($u'/U_{0,N} \sim 0.14$) shortly after the end of the potential core. Further downstream, the $u'/U_{0,N}$ values gradually decrease, indicative of the dissipation processes in decaying turbulence.

The behaviors of the controlled jets of Cases 1 and 2 are indicated in both time-averaged and fluctuating velocity components (Fig. 13a, b). The control effect of Cases 1 and 2 causes that the velocity on the axis starts to gradually decay immediately downstream the nozzle exit (Fig. 13a). In other words, no region of constant velocity can be observed, indicating that the potential core is suppressed. Moreover, Fig. 13a shows that the differences in the time-averaged velocities of the controlled jets of Cases 1 and 2 are very small.

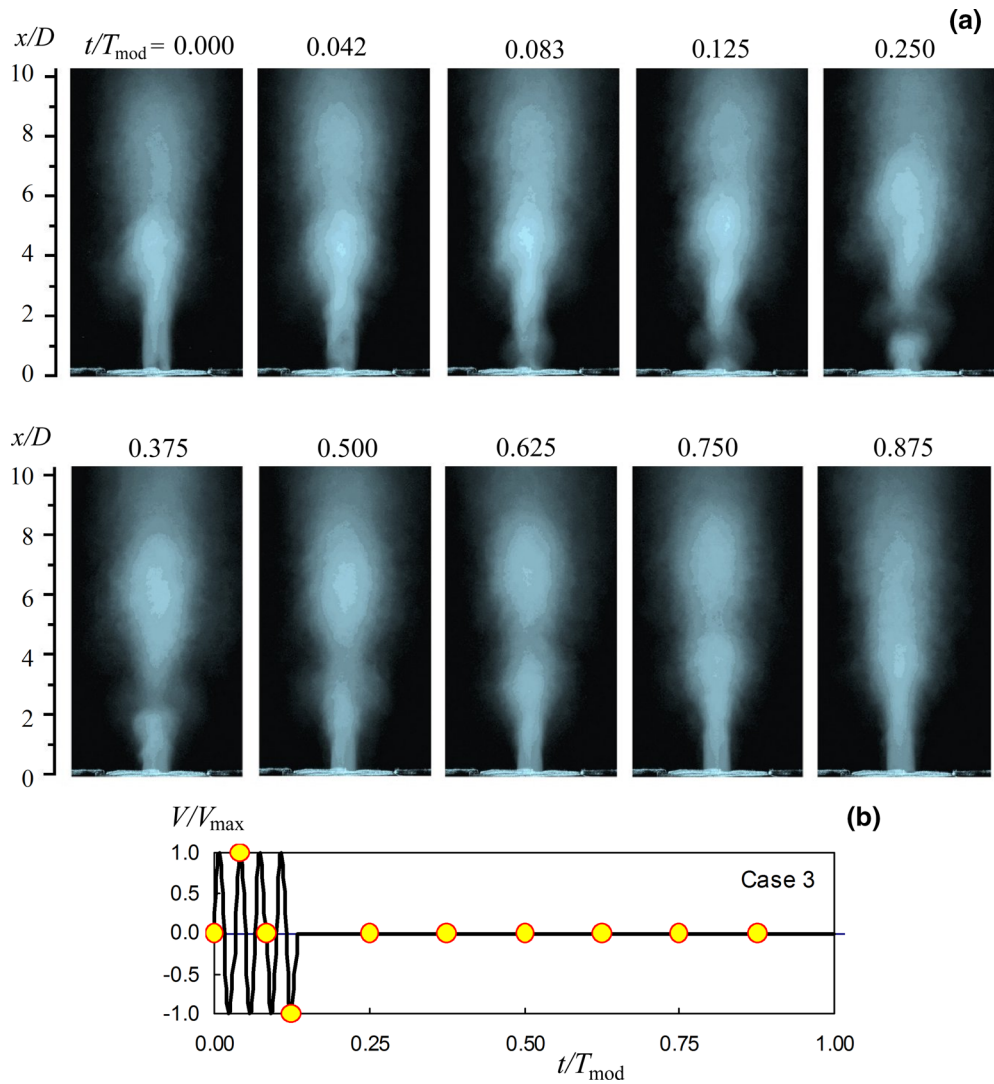


Fig. 11 **a** Phase-locked visualization during the actuating cycle for Case 3; parameters are summarized in Table 1; **b** driving signal with marks indicating phases of the visualizations

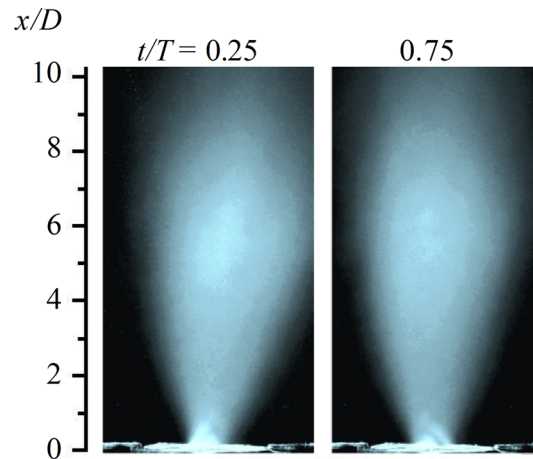


Fig. 12 Phase-locked visualization during the actuating cycle for Case 4; parameters are summarized in Table 1

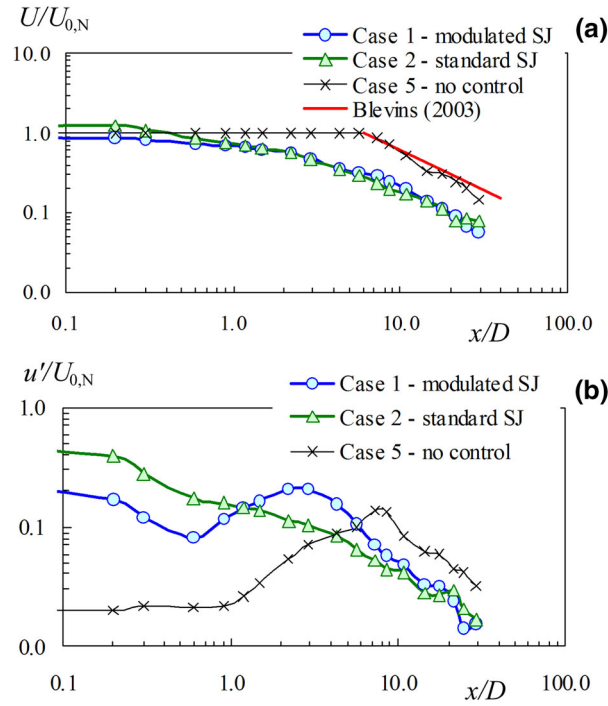


Fig. 13 Evolution of the velocity along the axis ($r = 0$) for Cases 1, 2, and 5; **a** time-averaged velocity component, **b** fluctuating velocity component

Figure 13b shows the massive increase in the velocity fluctuations at the nozzle exit for both of the controlled jets of Cases 1 and 2 in comparison with the unforced jet, Case 5, with $u'/U_{0,N} = 0.20$ and 0.40 for Cases 1 and 2 at the nozzle, respectively. Further downstream, developments of the fluctuations of both

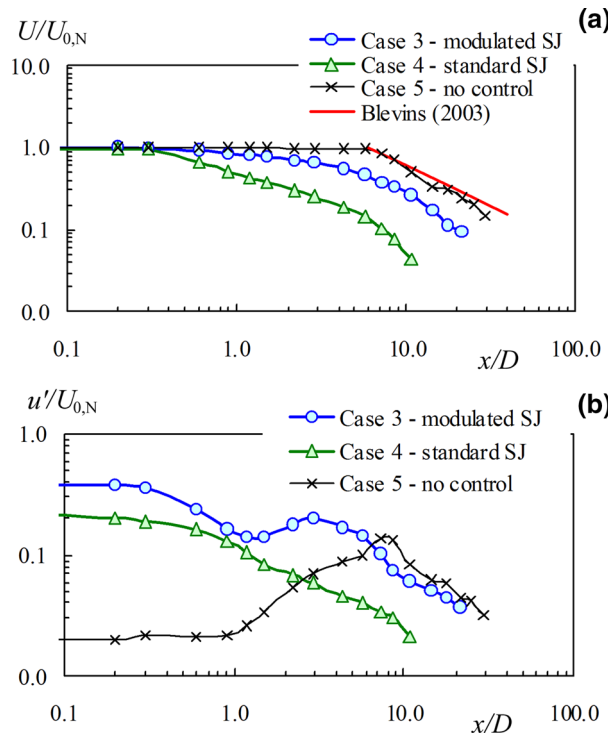


Fig. 14 Evolution of the velocity along the axis ($r = 0$) for Cases 3, 4, and 5; **a** time-averaged velocity component, **b** fluctuating velocity component

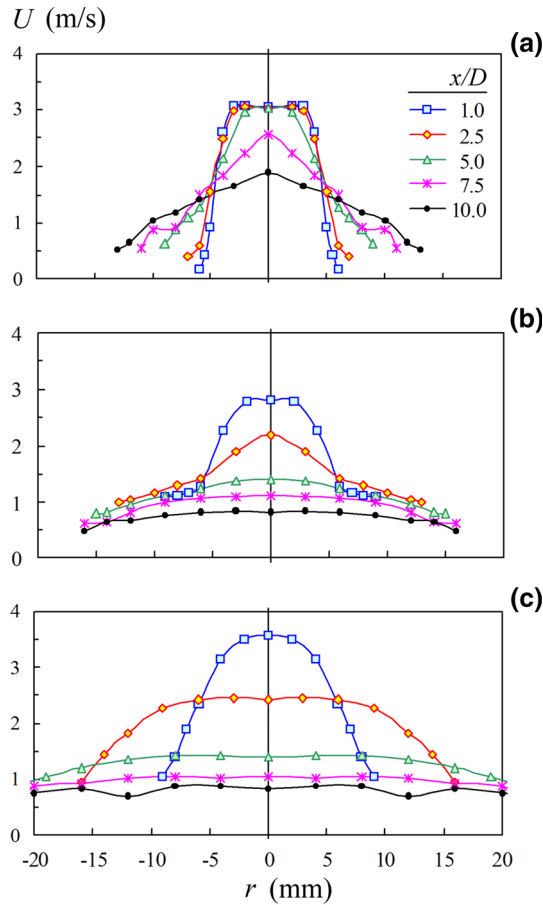


Fig. 15 Cross-stream velocity profiles of the time mean velocity for **a** reference unforced Case 5, **b** Case 1, **c** Case 2

of the controlled jets are different. For Case 1, the non-monotonic shape of the curve in Fig. 13b resembles that of the unforced jet (Case 5) with a typical local maximum of $u'/U_{0,N}$. However, the local maximum for Case 1 occurs much sooner, namely $u'/U_{0,N} = 0.21$ at $x/D = 2-3$. On the other hand, Case 2 presents a monotonic decrease over the entire test section, in the absence of any local maximum.

Figure 14a, b shows the jet evolution for higher-frequency control (Cases 3 and 4). In principle, the jet behavior is similar to that described in Fig. 13a, b. Again, the control effect causes the potential core of the main jet to be suppressed (Fig. 14a) while the $u'/U_{0,N}$ at the nozzle is massively increased (Fig. 14b). On the other hand, a comparison of the results for Cases 3 and 4 in Fig. 14a indicates much bigger differences than observed in Fig. 13a. Figure 14a shows that the standard control SJ (Case 4) causes a much steeper velocity decay than the modulated SJ of Case 3.

The influence of the active control can be assessed also via the jet velocity profiles. Figure 15a shows the time-averaged streamwise velocity profiles of the main unforced jet (Case 5) at several distances from the nozzle exit. The profiles at the nozzle exit are flat, with a relatively thin boundary layer (top-hat velocity profiles). With increasing distance x , the width of the shear layer increases and the potential core, visible as a region of constant velocity around the axis, gradually diminishes. In accordance with the velocity decay (Fig. 13a), the velocity core is visible to a distance of approximately $x/D = 5$.

The control jets give rise to a different shape for the time-averaged velocity profiles. Figure 15b, c presents the effects of the modulated SJ and standard SJs of Cases 1 and 2, respectively. Due to the control effect of both cases, the region of constant velocity around the jet axis (potential core) is fully suppressed. With increasing distance, the velocity gradually decreases and the profiles widen. A comparison of Fig. 15a–c, i.e., the unforced Case 5 and controlled Cases 1 and 2, demonstrates an intensification of the velocity decay resulting from the control effect.

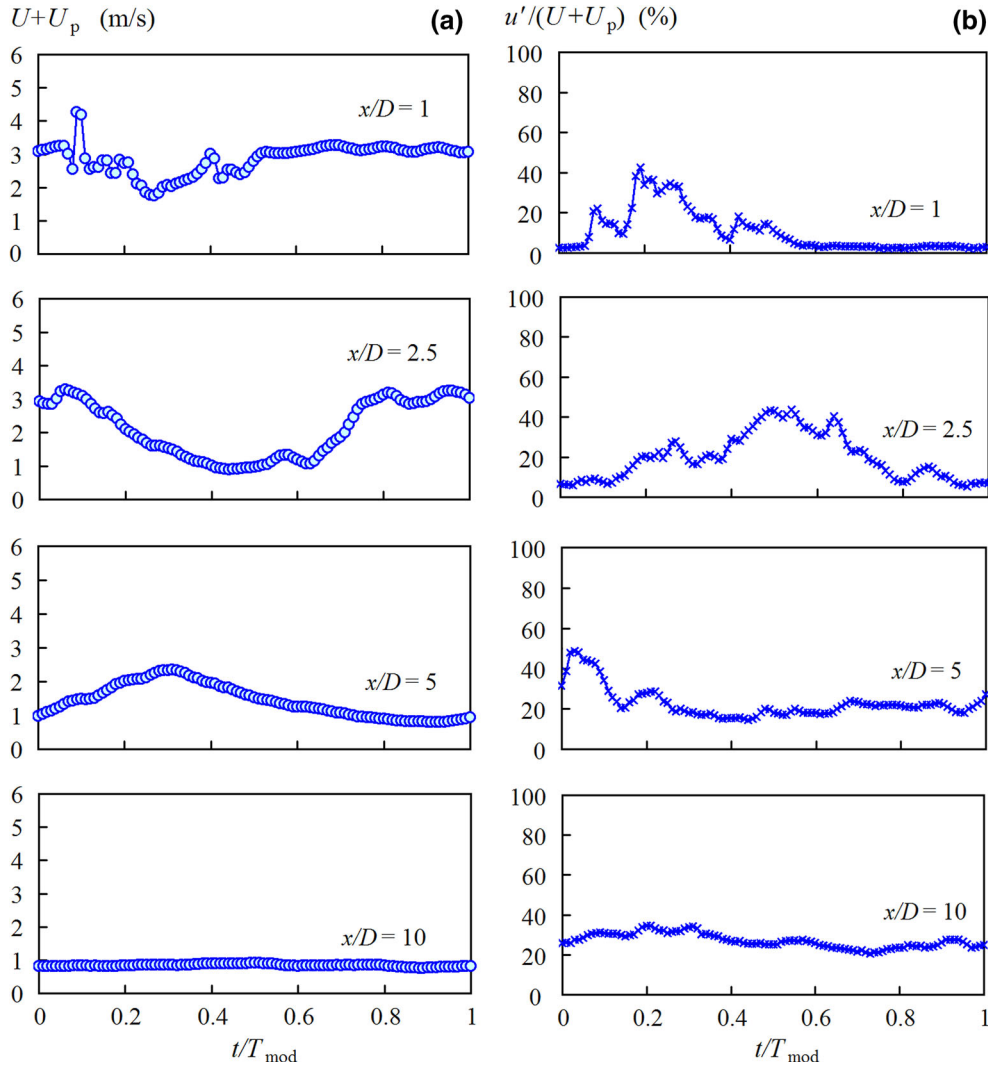


Fig. 16 Phase-averaged cycles of Case 1; **a** velocity along the axis, **b** velocity fluctuations at the same points

3.4 Intermittency of the jet flow

Figures 16 and 17 show the phase-averaged components of the centerline velocity during the operating cycle for the control jets of Cases 1 and 3, respectively. Figure 16a illustrates the development of the cycle shape as well as the decrease in the overall level and diminishing of its maximum at $x/D = 1$ –10. At the nozzle exit ($x/D = 1$), the velocity peak at $t/T_{\text{mod}} = 0.1$ indicates the pulse of the control signal. Further downstream, at $x/D = 2.5$ –5, the velocity cycle oscillates greatly between the lower and higher levels. The ratio of the velocity magnitudes at these levels varies from 2.5 to 3.5 at $x/D = 2.5$. Further downstream, at $x/D = 10$, the velocity decreases and the cycle becomes smoother. This is associated with a decay of the structures from the control process and agrees with flow visualization shown in Fig. 9, because the jet flapping does not reach the region of $x/D = 10$.

The dimensionless velocity fluctuations are plotted in Fig. 16b as the ratio of the components of $u'/(U + U_p)$. At the nozzle orifice ($x/D = 1$), the peaks in the velocity fluctuations at $t/T_{\text{mod}} = 0.1$ –0.2 indicate the control signal pulse, while relatively large parts of the cycle at $t/T_{\text{mod}} = 0$ –0.06 and 0.57–1 exhibit very low velocity fluctuations, at less than 4%. This effect, together with the periodicity of the velocity cycle, indicates the intermittent character of the jet flow. The periodicity of the fluctuation cycle is easily distinguished up to $x/D = 5$. Further downstream, at $x/D = 10$, the peak of the fluctuation cycle is hardly noticeable, which is associated with the smoothing of the cycle and decay of the jet.

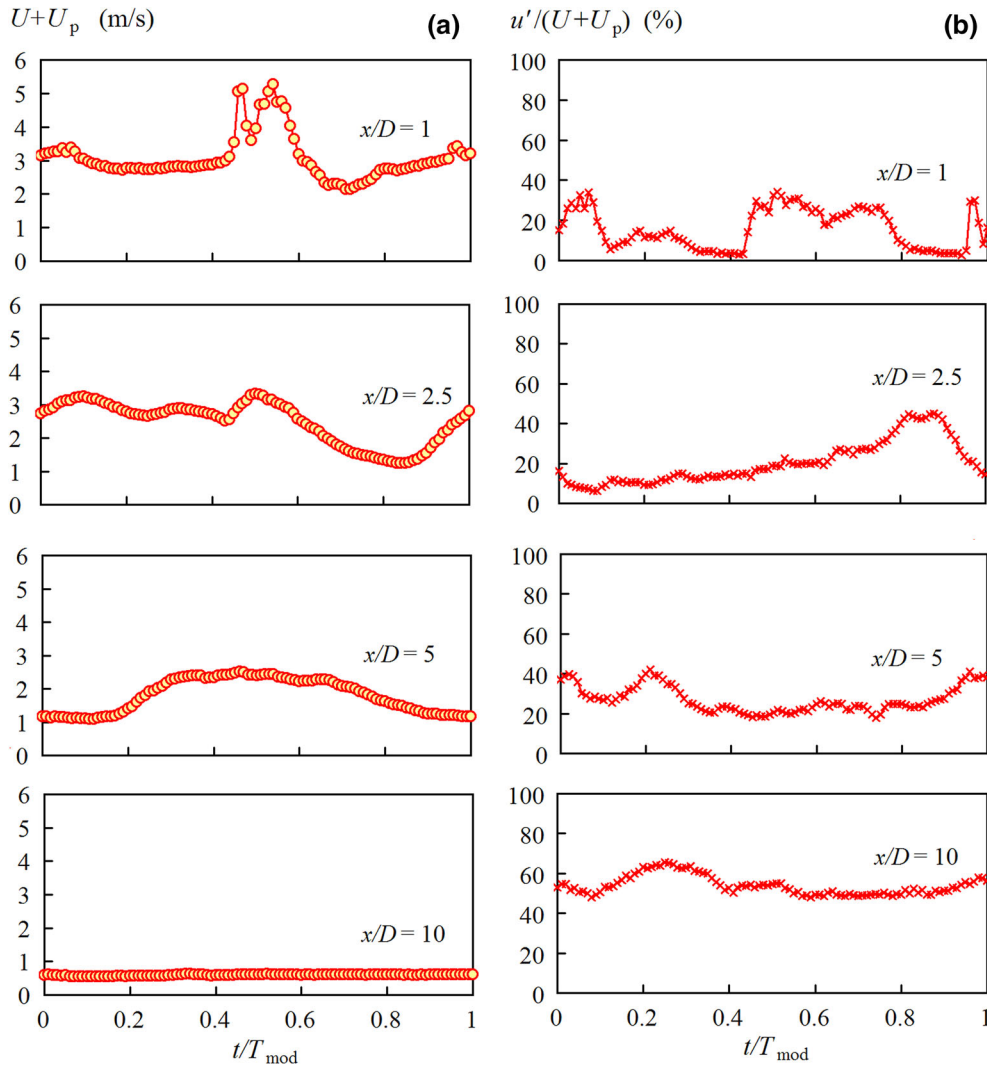


Fig. 17 Phase-averaged cycles of Case 3; **a** velocity along the axis, **b** velocity fluctuations at the same points

Similar to the results for Case 1 discussed in Fig. 16, the phase-averaged velocity components for the higher-frequency actuation of Case 3 are shown in Fig. 17. Again, an intermittent flow character is indicated by a periodicity of both the phase-averaged and fluctuating velocity components shown in Fig. 17a, b. The periodicity is distinguishable up to a distance of $x/D \leq 5$. Moreover, at the nozzle orifice ($x/D = 1$), the level of the velocity fluctuations oscillates widely between a low level of about 3–4% and a higher level of $26 \pm 8\%$. Further downstream, at $x/D = 10$, the phase-averaged velocity component is very weak (about 0.5–0.6 m/s) and the cycle becomes smooth. The decay of the jet flow and its periodicity is more intensive than for Case 1, which agrees with another manifestation of a very intensive jet decay caused by Case 3 control, as presented in Figs. 13 and 14.

4 Conclusions

An axisymmetric air jet was actively controlled using a pair of lateral control jets, which were generated by a pair of opposing synthetic jet actuators based on electrodynamic transducers (loudspeakers). The control signal was a pulse-modulated sinusoidal one. Two carrier frequencies were tested, namely 160 Hz and 840 Hz. These frequencies were chosen to be near the first and second resonances of the actuators, which were experimentally evaluated for this purpose. The duty cycle was chosen as 12–13%. The combination of

these parameters yielded four variants of the control signal, which were tested, which are given in Table 1: Cases 1 and 3 used pulse-modulated control signals, while Cases 2 and 4 used an un-modulated sinusoidal signal of the same frequencies as the mentioned carrier frequencies. As the reference case, an unforced continuous jet (Case 5) was used. For all of the investigated cases, the Reynolds number of the main axisymmetric jet was adjusted to be $Re = 1570$.

The experimental investigation used flow visualization and hot-wire anemometry. The first step focused on the behavior of single control jets; thus, these experiments were performed without the main jet. The hot-wire measurements quantified the velocity cycles and revealed interactions of the control jets and their reflections from the opposite nozzle walls. The characteristic velocities of the control synthetic jets were evaluated as $U_0 = 2.0\text{--}3.7$ m/s. For the case of pulse-modulated jets, the duty cycle effect causes a proportional reduction of the characteristic velocities to $U_{0,\text{mod}} = 0.2\text{--}0.5$ m/s.

The second step of the experiments investigated the main jet with the control effects. In general, all tested control cases caused a suppression of the jet core and more rapid jet flow decay; thus, the time-averaged velocity decrease occurred immediately at the nozzle exit. For the cases with the pulse-modulated control signal, the resulting controlled jets were intermittent in character. Depending on the carrier frequency, two different cases were observed:

- For the lower carrier frequency of 160 Hz, the pulse modulation caused a flip–flop motion of the jet, creating a zigzag pattern of the jet. Periodicities of the time-averaged and fluctuation velocity components were distinguished up to $x/D \leq 5$. Further downstream, at $x/D = 10$, the periodicity was hardly noticeable, which is associated with smoothing of the cycle and decay of the jet.
- For the higher carrier frequency of 840 Hz, the pulse modulation does not cause jet flapping with a zigzag pattern. Nevertheless, the periodicities of the time-averaged and fluctuation velocity components were distinguishable up to $x/D \leq 5$.

The present study demonstrates the possibility of generating intermittent jet flows by means of a pair of lateral pulse-modulated synthetic jets, with no mechanically movable elements in the test section. As was demonstrated by the short bibliographic overview in “Introduction,” intermittent jets are considered to be profitable tools for use in various industrial applications, typically those focusing on heat and mass transfer enhancement.

Acknowledgements We gratefully acknowledge the support of the Grant Agency of the Czech Republic—Czech Science Foundation (project no. 16-16596S) and the institutional support RVO: 61388998.

References

- Azevedo LFA, Webb BW, Queiroz M (1994) Pulsed air jet impingement heat transfer. *Exp Therm Fluid Sci* 8:206–213
- Bejan A (1995) *Convection heat transfer*, 2nd edn. Wiley, New York
- Ben Chiekh M, Bera JC, Sunyach M (2003) Synthetic jet control for flows in a diffuser: vectoring, spreading and mixing enhancement. *J Turbul* 4:1–12
- Blevins RD (2003) *Applied fluid dynamics handbook*. Krieger Publishing Company, Malabar
- Broučková Z, Trávníček Z (2015) Visualization study of hybrid synthetic jets. *J Vis* 18:581–593
- Camci C, Herr F (2002) Forced convection heat transfer enhancement using a self-oscillating impinging planar jet. *J Heat Transf Trans ASME* 124:770–782
- Cater JE, Soria J (2002) The evolution of round zero-net-mass-flux jets. *J Fluid Mech* 472:167–200
- Crow SC, Champagne FH (1971) Orderly structure in jet turbulence. *J Fluid Mech* 48:547–591
- De Luca L, Girfoglio M, Coppola G (2014) Modeling and experimental validation of the frequency response of synthetic jet actuators. *AIAA J* 52:1733–1748
- Durst Heim U, Ünsal B, Kullik G (2003) Mass flow rate control system for time-dependent laminar and turbulent flow investigations. *Meas Sci Technol* 14:893–902
- Favre-Marinet M, Binder G, Hac TV (1981) Generation of oscillating jets. *J Fluids Eng Trans ASME* 103:609–614
- Feero MA, Lavoie P, Sullivan PE (2015) Influence of cavity shape on synthetic jet performance. *Sens Actuator A Phys* 223:1–10
- Glezer A, Amitay M (2002) Synthetic jets. *Annu Rev Fluid Mech* 34:503–529
- Haneda Y, Tsuchiya Y, Nakabe K, Suzuki K (1998) Enhancement of impinging jet heat transfer by making use of mechano-fluid interactive flow oscillation. *Int J Heat Fluid Fl* 19:115–124
- Herwig H, Mocikat H, Gürtler T, Göppert S (2004) Heat transfer due to unsteadily impinging jets. *Int J Therm Sci* 43:733–741
- Hill WG Jr, Greene PR (1977) Increased turbulent jet mixing rates obtained by self-excited acoustic oscillations. *J Fluids Eng Trans ASME* 99:520–525
- Hsiao FB, Chou YW, Huang JM (1999) The study of self-sustained oscillating plane jet flow impinging upon a small cylinder. *Exp Fluids* 27:392–399
- Hussain AKMF, Hasan MAZ (1983) The ‘whistler nozzle’ phenomenon. *J Fluid Mech* 134:431–458

- Kordík J, Trávníček Z (2017) Optimal diameter of nozzles of synthetic jet actuators based on electrodynamic transducers. *Exp Therm Fluid Sci* 86:281–294
- Kordík J, Trávníček Z (2018) Non-harmonic excitation of synthetic jet actuators based on electrodynamic transducers. *Int J Heat Fluid Fl* 73:154–162
- Kordík J, Broučková Z, Vít T, Pavelka M, Trávníček Z (2014) Novel methods for evaluation of the Reynolds number of synthetic jets. *Exp Fluids* 55:1757-1–1757-16
- Mi J, Nathan GJ, Luxton RE (2001) Mixing characteristics of a flapping jet from a self-exciting nozzle. *Flow Turbul Combust* 67:1–23
- Mladin EC, Zumbrunnen DA (1997) Local convective heat transfer to submerged pulsating jets. *Int J Heat Mass Tran* 40:3305–3321
- Mohseni K, Mittal R (2015) *Synthetic Jets: Fundamentals and Applications*. CRC Press, Boca Raton
- Nathan GJ, Hill SJ, Luxton RE (1998) An axisymmetric ‘fluidic’ nozzle to generate jet precession. *J Fluid Mech* 370:347–380
- Pack LG, Seifert A (2001) Periodic excitation for jet vectoring and enhanced spreading. *J Aircr* 38:486–495
- Page RH, Chinnock PS, Seyed-Yagoobi J (1996) Self-oscillation enhancement of impingement jet heat transfer. *J Thermophys Heat Transf* 10:380–382
- Qayoum A, Gupta V, Panigrahi PK, Muralidhar K (2010) Influence of amplitude and frequency modulation on flow created by a synthetic jet actuator. *Sens Actuator A Phys* 162:36–50
- Raman G, Rice EJ, Cornelius DM (1994) Evaluation of flip-flop jet nozzles for use as practical excitation devices. *J Fluids Eng-Trans ASME* 116:508–515
- Reynolds WC, Parekh DE, Juvet PJD, Lee MJD (2003) Bifurcating and blooming jets. *Annu Rev Fluid Mech* 35:295–315
- Smith BL, Glezer A (1998) The formation and evolution of synthetic jets. *Phys Fluids* 10:2281–2297
- Smith BL, Glezer A (2002) Jet vectoring using synthetic jets. *J Fluid Mech* 458:1–34
- Tamburello DA, Amitay M (2007a) Interaction of a free jet with a perpendicular control jet. *J Turbul* 8(21):1–27
- Tamburello DA, Amitay M (2007b) Dynamic response of a free jet following the activation of a single synthetic jet. *J Turbul* 8(48):1–18
- Thomas FO (1991) Structure of mixing layers and jets. *Appl Mech Rev* 44:119–153
- Trávníček Z, Peszyński K, Hošek J, Wawrzyniak S (2003) Aerodynamic and mass transfer characteristics of an annular bistable impinging jet with a fluidic flip-flop control. *Int J Heat Mass Transf* 46:1265–1278
- Trávníček Z, Němcová L, Kordík J, Tesař V, Kopecký V (2012) Axisymmetric impinging jet excited by a synthetic jet system. *Int J Heat Mass Transf* 55:1279–1290
- Trávníček Z, Tesař V, Broučková Z, Peszyński K (2014) Annular impinging jet controlled by radial synthetic jets. *Heat Transf Eng* 35:1450–1461
- Viets H (1975) Flip-flop jet nozzle. *AIAA J* 13:1375–1379
- Zhang PF, Wang JJ (2007) Novel signal wave pattern for efficient synthetic jet generation. *AIAA J* 45:1058–1065
- Zumbrunnen DA, Aziz M (1993) Convective heat-transfer enhancement due to intermittency in an impinging jet. *J Heat Transf Trans ASME* 115:91–98